Energy Conversion and Management 85 (2014) 718–726

Contents lists available at ScienceDirect

Energy Conversion and Management

journal homepage: www.elsevier.com/locate/enconman

Study on a basic unit of a double-acting thermoacoustic heat engine used for dish solar power

S. Zhang [a,b], Z.H. Wu [a], R.D. Zhao [a,b], G.Y. Yu [a], W. Dai [a], E.C. Luo [a,*]

[a] Key Laboratory of Cryogenics, Chinese Academy of Sciences, Beijing 100190, China
[b] University of Chinese Academy of Sciences, Beijing 100049, China

ARTICLE INFO

Article history:
Available online 25 March 2014

Keywords:
Dish-solar power
Double-acting
Thermoacoustic heat engine

ABSTRACT

A double-acting thermoacoustic heat engine was invented recently by our group. It generally consists of several sequentially connected identical units. In order to apply such a system to dish-solar power generation and for better absorbing concentrated solar heat, a special-shaped heater composed of a bundle of tubes was designed. To understand the internal operating mechanism and thermodynamic performance of such a solar-driven thermoacoustic generator, a test rig having only one basic unit was designed, built and tested. Firstly, thermoacoustic conversion performance of this test rig was theoretically predicted based on linear thermoacoustic model. By adjusting the external resistance and moving mass of the expansion motor, the acoustic filed in the THE can be regulated to fulfil better energy conversion. In the simulation, a highest thermal efficiency of 51.37% and a net acoustic power of 1.6 kW under a heating temperature of 650 °C can be obtained. Then, the experiments were conducted and compared with the simulation results. A discrepancy between the theoretical and experimental results was observed and discussed, and guidance was given to improve the experimental system.

© 2014 Elsevier Ltd. All rights reserved.

1. Introduction

Solar energy is the most abundant clean energy on earth. A great portion of solar energy impinging on earth is thermal radiation. However, the efficient and reliable way to use this part of solar energy is very limited. Thermoacoustic heat engines (THE) can effectively convert solar energy to acoustic power, i.e. mechanical energy, based on the thermoacoustic effect, such as the Rijke and Sondhauss effect. THEs also have some other great advantages. First, a THE generally consists of several heat exchangers, regenerator or stack and tubes, which means there are no moving components in high temperature parts, so THEs are more reliable and with a long life-time. Second, THEs are generally charged with inert gases such as helium and nitrogen, hence they are environmentally friendly. Third, in addition to solar energy, THEs can also use other low-grade energy such as waste heat. A comprehensive review of THEs was presented by Swift in 1988 [1]. The mechanism of THE can be understood based on the interaction between solid and gas particles. When heat is supplied through the hot end heat exchanger and the ambient heat exchanger is cooled, the temperature gradient along the regenerator or stack is established. The gas particle interacts with solid materials (stack or regenerator) and when the temperature gradient is large enough the oscillation occurs, realizing the enlarging or generation of acoustic power, i.e. mechanical energy. With the increasing concern of high efficient energy conversion and the utilization of low-grade energy, the researches of thermoacoustic heat engines (THE) are booming in recent decades.

There are two typical kinds of THEs — the standing wave ones and the travelling wave ones. The latter operates based on the Stirling Cycle which has the potential of high efficiency [2]. The first concept of travelling wave THE was proposed by Ceperley in 1979 [3], and later in 1998 Yazaki et al. built a modified THE based on Ceperley's work [4]. But their THEs had a serious problem of large viscous loss in the regenerator or stack. A breakthrough of travelling wave THE was made in 1999 when Backhaus and Swift [5] developed a travelling wave THE with a thermal efficiency of 30%. In 2005, Luo et al. [6] proposed an energy-focused travelling wave THE which contained a tapered resonance tube to reduce the nonlinear dissipation in the resonance tube and the pressure ratio reached 1.4. In 2010, Kees de Blok proposed a novel 4-stage travelling wave THE [7]. The multi-stage configuration is beneficial for even higher energy density and larger power capacity. There are also some real applications for THEs. Since 1994, a project focusing on the application to natural gas liquefier driven by THE has been conducted [8]. A thermoacoustic generator for

* Corresponding author. Tel./fax: +86 10 82543750.
E-mail address: ecluo@mail.ipc.ac.cn (E.C. Luo).

http://dx.doi.org/10.1016/j.enconman.2014.02.065
0196-8904/© 2014 Elsevier Ltd. All rights reserved.

Nomenclature

Abbreviation

THE	thermoacoustic heat engine
1-D	one dimension

Symbols

a	speed of sound, m/s
A	area, m^2
B	magnetic field, T
c	heat capacity per unit mass, J/kg K
D	diameter, m
E	acoustic power, W
f	frequency, Hz
f	spatially averaged diffusion function
$\dot{H}$	total energy power, W
i	$\sqrt{-1}$, imaginary unit
I	input current, A
k	thermal conductivity, W/m K
K	spring constant, N/m
l	length, m
L	electrical inductance, H
M	mass of piston, kg
p	pressure amplitude, MPa
P	working pressure, MPa
$\dot{q}$	heat input per unit length, W/m
Q	heat transferred, W
R	electrical resistance, Ω
R	mechanical resistance, N s/m
T	temperature, K
U	volume flow rate, m^3/s
V	input voltage, V
Z	impedance, Pa s/m^3

Greek symbols

γ	specific heat ratio
δ	penetration depth, m
θ	phase delay, °
ξ	correction factor of channel solid thermal parameters
ρ	gas density, kg/m^3
σ	Prandtl number
τ	transduction coefficient
ω	angular frequency, s^{-1}
Re []	real part of
Im []	imaginary part of
$\sim$	conjugation of a complex quantity
| |	amplitude of a complex quantity

Subscript

1	first order
2	second order
e	electrical
m	mean
m	mechanical
p	isobaric
s	solid
κ	thermal
v	viscous
com	compressor
gen	expansion motor
in	input
in	inlet
net	net
out	outlet

applications such as LED lightening or charging battery driven by waste heat from stove has been constructed recently [9]. However, the above-mentioned THEs have a common problem of having a long resonant tube, which has limited the further application of THEs. Thus, in recent time our research group has presented a concept of double-acting multi-cylinder travelling wave THE [10] to solve the problem. It is schematically shown in Fig. 1. This engine mainly consists of several sequentially connected basic units in a closed loop. Each basic unit is composed of main components of a THE sandwiched by the compression and expansion pistons. "Double-acting" means one piston works as compression piston to the previous THE unit and simultaneously as expansion piston to the last unit. This novel configuration not only has the traditional advantages of THEs but also some other advantages as stated below. This double-acting THE is capable of producing larger power because of its multi-cylinder configuration. In addition, several symmetric units cascading in one loop is equivalent to several THEs working together, hence the configuration is relatively compact. Taking advantages of high inertia of the pistons this configuration also eliminates the long resonant tube. Recently, we are considering constructing a double-acting THE for dish-solar power generation, aiming at a 5 kW acoustic power output which is for used to drive electric expansion motors. In order to effectively absorb the concentrated solar heat, a special-shaped heater composed of a bundle of tubes was designed. Different from the generally-used shell-and-tube and plate-fin heat exchangers, this heater has much longer and less tubes and the shape is irregular which will result in problems of jet-flow and turbulence. The whole system is complicated, but it consists of several symmetric units which mean each basic unit should have the same performance. Hence in order to study the advantages as well as drawbacks, and find ways to improve it, a test rig having only one basic unit which is representative to the system was designed, built and tested. Firstly, a numerical analysis was carried out to study the thermal conversion performance. Then experiments

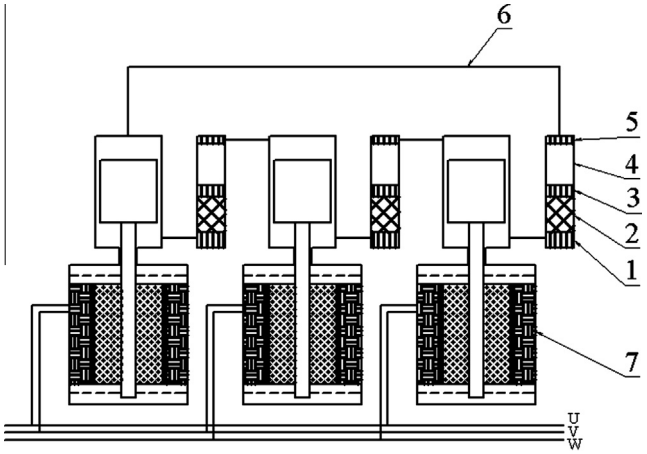

1- main ambient heat exchanger; 2-regenerator; 3-heater;
4-thermal buffer tube; 5-secondary ambient heat exchanger
6-connection tubes; 7- motor

Fig. 1. Schematic of double-acting THE.

were conducted and compared with the simulation results. Finally, conclusions were made.

2. Test rig

Fig. 2 is an assembly drawing of a 6 × 1 kW double-acting THE used for dish solar power generation. This 6 × 1 kW double-acting THE consists of two 3 × 1 kW double-acting THEs, and the two sub-systems are carefully arranged to minimize the vibration. The top part of the system is a heater composed of a bundle of tubes. This configuration is beneficial for absorbing concentrated solar heat.

Since the configuration is complicated, a test rig having only one basic unit is built to understand the internal operating mechanism. The schematic diagram of the test unit is shown in Fig. 3. The test unit consists of a compression motor, a THE and an expansion motor. The THE consists of a main ambient heat exchanger, regenerator, heater, thermal buffer tube and secondary ambient heat exchanger. The compression motor and expansion motor are both of dual-opposed configurations. The two pistons of each motor move in the opposite direction and since their same configurations and same mass the vibration is reduced based on the conservation of momentum. The compression motor and expansion motor are working simultaneously to modulate the acoustic field. The acoustic power is input from the compression motor, amplified in the tested THE unit and then consumed in the expansion motor.

Consequently the net acoustic power E_{net} generated in the tested THE unit is:

$$E_{net} = E_{gen} - E_{com} \tag{1}$$

where E_{gen} is the acoustic power consumed in expansion motor and E_{com} is the acoustic power input from the compression motor.

And the thermal efficiency of the tested THE unit is:

$$\eta = \frac{E_{net}}{Q_{in}} \times 100\% \tag{2}$$

where Q_{in} is the heat input in the heater.

The impedance of motor can be described as:

$$Z = \frac{U_1}{P_1} = \frac{1}{A^2}\left[R_m + i\left(\omega m - \frac{K}{\omega}\right) + \frac{\tau^2}{R_e + i(\omega L - 1/\omega C)}\right] \tag{3}$$

Fig. 2. A 6 × 1 kW double-acting THE used for dish solar power.

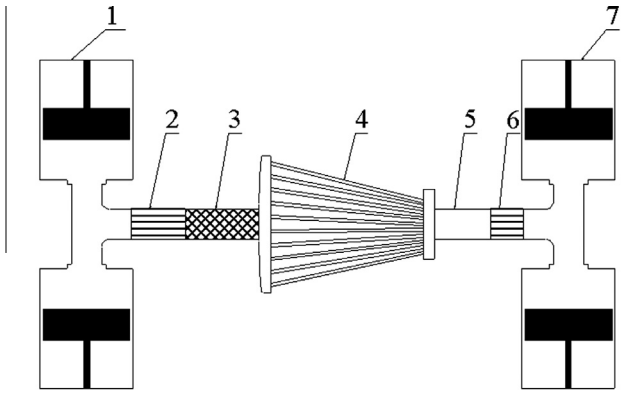

1- compression motor; 2- main ambient heat exchanger;
3- regenerator; 4- heater; 5- thermal buffer tube;
6- secondary ambient heat exchanger; 7- expansion motor

Fig. 3. Schematic of a basic unit of a double-acting THE used for dish solar power generation.

where R_e is the electrical resistance, including the internal resistance, i.e. the resistance of the coil, and the external resistance.

The distribution of acoustic filed, which is determine to the acoustic power generated, can be mathematically reflected by the distribution of pressure amplitude P_1 and volume flow rate U_1, i.e. the product of oscillation velocity and gas flow area. According to Eq. (3), by adjusting the impedance of the expansion motor, we can obtain different acoustic distributions, hence the performance of the system under different acoustic conditions could be studied. Although many parameters of the motor can be adjusted to realize the adjutancy of impedance, the change of the external resistance R and mass of the piston M is most convenient. Consequently, in the following studies, we adjust these two parameters to establish different acoustic conditions to study the acoustic power generation in the tested THE unit.

Table 1 gives the dimensions of the tested THE unit. Table 2 gives the parameters of the compression motor and expansion motor. These dimensions are coincident in the 6 × 1 kW system, the numerical model and the test rig. Since the compression motor and the expansion motor each have two same pistons, only one single piston's parameters are given.

3. Simulation analysis

3.1. Simulation model

Based on the linear thermoacoustic theory, the simulation is conducted using the DeltaEC 6.2 program [11]. This program provides many segments including pipe, regenerator, heat exchanger, etc. for users to simulate different components of a thermoacoustic system. The program integrates the governing equations in one dimension (1-D). The geometry parameters are given by the user. And the thermophysical properties of gas and solid are given in the DeltaEC's library. A shooting method is introduced in the program to satisfy various boundary conditions set by the users.

3.1.1. Geometric model

The simulation model is based on the construction of the basic unit, but some simplification has been made, as seen in Fig. 4. Firstly, the real compression motor is dual-opposed, and the electric circuits of the two pistons are in parallel. In the simulation, we adopt only one piston which is equivalent to the two paralleled pistons. Hence, the cross-sectional area of this equivalent piston is the sum of the two pistons' areas. And other parameters of the equivalent piston equal to the sum of the corresponding

Table 1
Dimensions of tested THE unit.

	D (mm)	l (mm)	Others
Main ambient heat exchanger	55	52	Shell-and-tube heat exchanger 241 tubes with 1.5 mm inner diameter
Regenerator	55	40	150 mesh stainless steel screen
Heater	2	210	19 tubes
Thermal buffer tube	38	120	/
Secondary ambient heat exchanger	38	30	Shell-and-tube heat exchanger 121 tubes with 1.5 mm inner diameter

Table 2
Parameters of compressor and generator (single piston).

	D (mm)	M (kg)	K (kN m^{-1})	R_m (N s m^{-1})	R_e (Ω)	Bl (N A^{-1})
Compressor	60	2.08	180	16	3.72	97.7
Generator	50	1.1	167.5	20	3.5	95

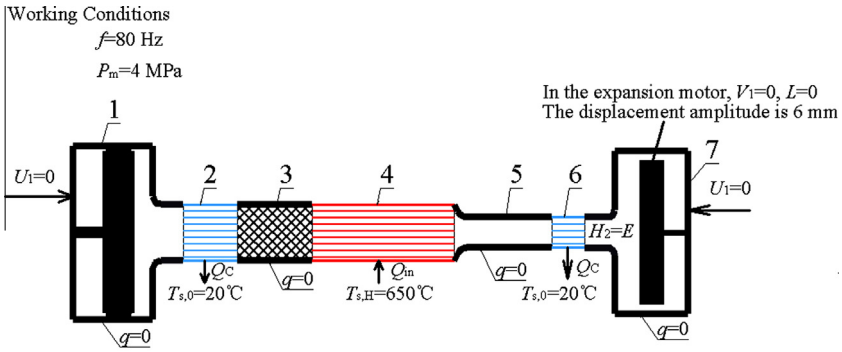

Fig. 4. Geometric model.

parameters of the two paralleled pistons. For the expansion motor, we adopt the same treatment. Secondly, we simplify the special-shaped heater into a shell-and-tube heat exchanger with an inner diameter of 55 mm and with 19 tubes whose inner diameter is 2 mm.

3.1.2. Governing equations

For the components charged with gas, based on the linear thermoacoustic theory [12], the governing equations are:

$$\frac{dp_1}{dx} = -\frac{i\omega\rho_m}{1-f_v}\frac{U_1}{A} \tag{4}$$

$$\frac{dU_1}{dx} = -\frac{i\omega A}{\gamma p_m}\left[1+\frac{(\gamma-1)f_\kappa}{1+\xi}\right]p_1 + \frac{(f_\kappa - f_v)}{(1-f_v)(1-\sigma)(1+\xi)} \times \frac{U_1}{T_m}\frac{dT_m}{dx} \tag{5}$$

$$\frac{d\dot{H}_2}{dx} = \dot{q} \tag{6}$$

where

$$\dot{H}_2 = \frac{1}{2}\mathrm{Re}\left[p_1\tilde{U}_1\left(1-\frac{f_\kappa-\tilde{f}_v}{(1-f_v)(1-\sigma)(1+\xi)}\right)\right] + \frac{\rho_m c_p|U_1|^2}{2A\omega(1-\sigma)|1-f_v|^2}\frac{dT_m}{dx}\mathrm{Im}\left[\tilde{f}_v + \frac{(\tilde{f}_\kappa-\tilde{f}_v)(1+\xi f_v/f_\kappa)}{(1+\xi)(1-\sigma)}\right] - (Ak+A_s k_s)\frac{dT_m}{dx}$$

where ω is angular frequency and $\omega = 2\pi f$, here the resonant frequency f is set as 80 Hz. f_v and f_κ are viscous function and thermal function. Other symbols are defined in Nomenclature in detail.

At the inlet of one segment, p_1, U_1, T_m equal to the outlet parameters of the previous segment. P_m is set to be 4.0 MPa. A, A_s are given uniquely in different segments which can be calculated from the dimensions given in Tables 1 and 2. $\dot{q}$ equals to 0 in the most of the segments except for the heat exchangers. In the heat exchangers, $\dot{q}$ are solved to meet the targets of the specific solid temperatures in the heat exchangers.

With the assumed values of p_1 and U_1, the acoustic power E can be calculated:

$$E = \frac{1}{2}\mathrm{Re}[p_1\tilde{U}_1] = \frac{1}{2}\mathrm{Re}[\tilde{p}_1 U_1] = \frac{1}{2}|p_1||U_1|\cos\theta \tag{7}$$

where θ is the phase difference between p_1 and U_1.

For the pistons, the VESPEAKER model is used. The governing equations are:

$$U_1 = U_{1,in} - \frac{\omega}{\rho_m a^2}\frac{\gamma-1}{1+\xi}\frac{\delta_\kappa}{2}Ap_{1,in} \tag{8}$$

$$p_{1,out} - p_{1,in} = \tau' I_1 - Z_m U_1 \tag{9}$$

$$V_1 = Z_e I_1 - \tau U_1 \tag{10}$$

$$Z_e = R_e + i\omega L \tag{11}$$

$$Z_m = R_m/A^2 + i(\omega M - K/\omega)/A^2 \tag{12}$$

$$\tau = -\tau' = Bl/A \tag{13}$$

where $U_{1,in}$ is the volume flow rate at the inlet of the VESPEAKER, $p_{1,out}$, $p_{1,in}$ are the pressure amplitudes at the outlet and inlet of the VESPEAKER, respectively. We balance L with an external electrical compliance, hence L is 0 here. For compression motor, V_1 is guessed to meet the target of the displacement amplitude of the expansion motor piston. For expansion motor, V_1 is 0.

3.1.3. Boundary conditions

The beginning of the simulation model is the back cavity of the compression motor; hence the inlet U_1 is 0. In the main and secondary ambient heat exchangers, the solid temperature is set as 20 °C. The solid temperature of the heater is 650 °C. We consider that the piston of the expansion motor is a thermally insulated model, so $H_2 = E$ at the inlet of the expansion motor. The piston displacement amplitude of the expansion motor is set as 6 mm to prevent the piston from hitting the cylinder due to the limitation of back cavity volume. The end of the simulation model is the back cavity of the expansion motor, the outlet U_1 is 0.

3.1.4. Shooting method

In the DeltaEC program, a shooting method is introduced in the program to satisfy various boundary conditions set by the users.

At the inlet of the simulation model, we set the values of pressure amplitude p_1, gas temperature T_m, the input voltage V_1 of the compression motor, and the phase angle of the input voltage of the compression motor as "guessed parameters" and give them initial values. By integrating the governing equations, the outlet parameters of the simulation model can be obtained. If the outlet parameters do not meet the targets, the guessed parameters will be modified and given to the inlet of the model again until the outlet parameters meet the target parameters.

3.2. Simulation results and discussion

3.2.1. The influence of external resistance and moving mass

The distribution of acoustic field is not only influenced by the geometry parameters of the THE but also largely affected by the impedance of the expansion motor. Based on the above analysis, we can regulate the acoustic filed by adjusting the external resistance and the moving mass of the expansion motor. In this section, we mainly study the performance of the basic unit when the external resistance and the moving mass are changed. Note that the following-mentioned "external resistance" is the resistance which has already been transformed to the resistance needed in the paralleled electric circuit in the experiments. The following-mentioned moving mass is the mass of a single piston. In the following simulations, the external resistance varies from 5.25 Ω to 110 Ω. When the external resistance is smaller than 5.25 Ω, a positive thermal efficiency and net acoustic power are unable to be obtained. Three specific moving masses are studied, i.e., 1.0 kg, 1.1 kg and 1.2 kg.

The phase difference of volume flow rates at the interfaces of the compressor piston and the expansion motor piston is dominant because it can reflects the acoustic filed distribution in the tested THE unit. The distribution of acoustic field will further influence the performance of the basic unit, especially the energy conversion. Fig. 5 illustrates the curves of the phase difference of volume flow rates at the interfaces of the compression motor piston and the expansion motor piston. As seen in the figure, both the moving mass and the external resistance have a significant influence on the phase difference of the volume flow rates. When the moving masses are 1.0 kg, 1.1 kg and 1.2 kg, the phase differences range from −100.74° to −139.09°, from −104.88° to −152.72° and from −108.93° to −160.73°, respectively.

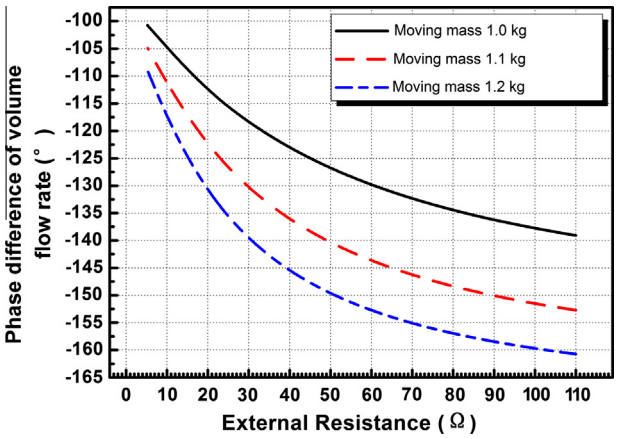

Fig. 5. External resistance versus phase delay of volume flow rate between pistons.

The net acoustic power generated and the thermal efficiency of the tested THE unit are the most important two parameters that imply the performance of the basic unit. An extremum of net acoustic power and thermal efficiency is obtained with suitable external resistance, which means the best acoustic field distribution has been obtained. When the external resistance is smaller than 10 Ω, the acoustic power generated in the tested THE unit abruptly jumps to the maximum value with only a bit increase of the external resistance, as shown in Fig. 6. With the further increase of the external resistance, the net acoustic power decreases smoothly. The external resistance versus thermal efficiency diagram has similar trend to that of the net acoustic power, as shown in Fig. 7. When the external resistance is smaller, the thermal efficiency increases dramatically to a maximum value with the increase of external resistance. Then the thermal efficiency has a slight decrease. However, the best acoustic field distribution is different to acoustic power and thermal efficiency. Hence the choice of external resistance should be compromised.

Similarly, there should also be a most suitable moving mass which will result in the extremum of net acoustic power and thermal efficiency. However, of the three moving mass we choose, i.e. 1.0 kg, 1.1 kg and 1.2 kg, the most suitable moving mass has not obtained yet.

Among the current moving mass and external resistance, the maximum acoustic powers generated are 1566.6 W, 1592.5 W and 1600.5 W with an external resistance of 10 Ω when the moving masses are 1.0 kg, 1.1 kg and 1.2 kg respectively. When the

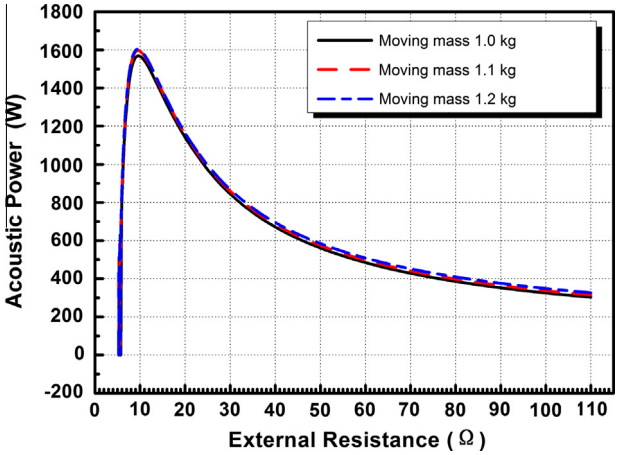

Fig. 6. External resistance versus acoustic power with different moving mass.

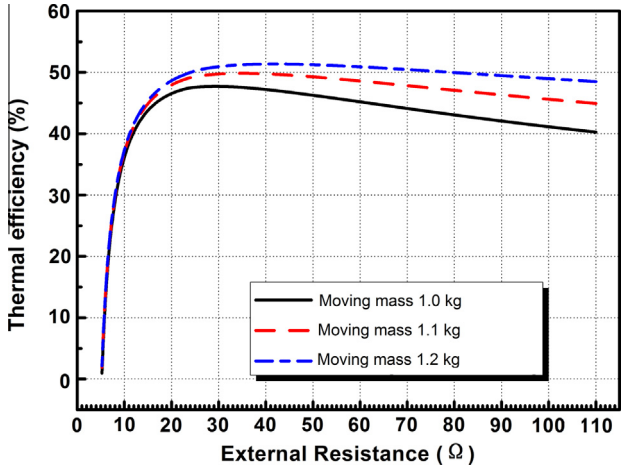

Fig. 7. External resistance versus thermal efficiency with different moving mass.

moving masses are 1.0 kg, 1.1 kg and 1.2 kg, the highest thermal efficiency of 47.72%, 49.81% and 51.37% are achieved with 29 Ω, 32 Ω and 42 Ω external resistances respectively.

In general, for a higher net acoustic power and thermal efficiency, a relatively smaller external resistance and a relatively higher moving mass is preferred.

3.2.2. The influence of heater

In this section, we mainly discuss the influences of the heater. The moving mass of the expansion motor is 1.1 kg and the external resistance is 32 Ω.

As mentioned above, the heater consists of 19 tubes with inner diameter of 2 mm. The influences of the number of tubes and tube diameters are very similar as they both determine the heat transfer area between gas and solid. Therefore, we only study the influence of the tube's inner diameter on the performance of the basic unit in this section. The inner diameter of the tube varies from 1 mm to 6 mm while the number of the tubes is fixed as 19. In the threshold of diameter, the phase difference varies from −147.39° to −128.76°, as shown in Fig. 8. The diameter of the heater tubes has a strong influence on the phase difference when the diameter is relatively small, i.e., smaller than 3 mm.

Fig. 9 demonstrates the influence of the diameter on net acoustic power generated in the tested THE unit and the thermal efficiency. When increasing the tube diameter, the heat transfer area increases. Hence the enhancement of heat transfer caused by the

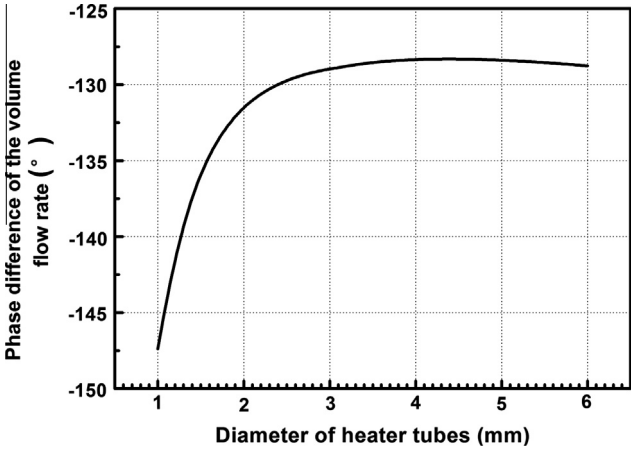

Fig. 8. Diameter of heater tubes versus phase difference of the volume flow rate.

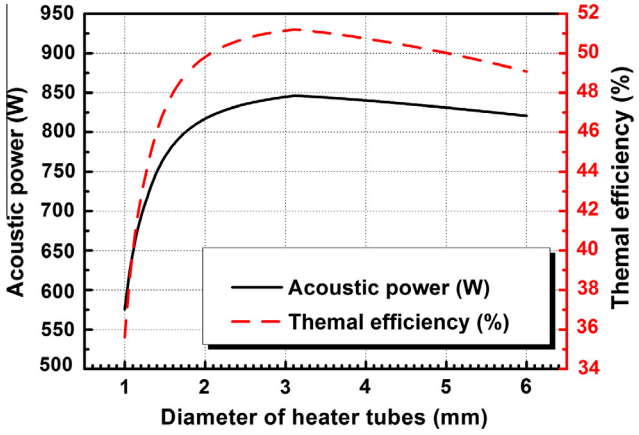

Fig. 9. Diameter of heater tubes versus acoustic power and thermal efficiency.

increase of heat transfer area will contribute to the increase of generated net acoustic power and thermal efficiency. However, as the diameter is larger than 3 mm, the surface viscous loss outweighs the heat transfer area, which results in the slight decrease of the net acoustic power and thermal efficiency. When the inner diameter of the tubes is 3.1 mm, the highest thermal efficiency of 51.19% and the maximum net acoustic power generated of 846.28 W have been achieved.

4. Experiment analysis

In this section, preliminary experiments were conducted and discussed. The experimental results are compared with the calculated results. Although there are still some issues left and the experimental results have much room for improvement, the fundamental trend of the experimental results is in reasonable agreement with the calculated results.

4.1. Experimental system

The implementation of the experimental system is shown in Fig. 10. Six silicon carbide heating rods are used for heat input. The rated power of each single silicon carbide heating rod is 800 W. Polycrystalline mullite is used for thermal insulation. The system is charged with 4.0 MPa helium and the resonant frequency is 80 Hz, which is the same as the simulation. A sheathed thermocouple is located at the surface of the heater on the regenerator side to measure the heater solid temperature. The heater solid temperature is set as 650 °C approximately. The temperature of

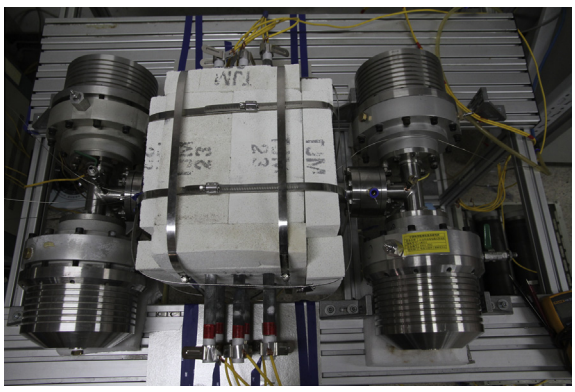

Fig. 10. Experimental system with heat insulator.

the gas in the heating chamber surrounded by the Polycrystalline mullite and the solid temperature of the hot end of the regenerator are measured to estimate the heat leakage. The pressures of the back and front cavity of the compressor and the expansion motor are measured.

4.2. Experimental results and discussion

A preliminary experiment is conducted and the results are compared with the simulation results in this section. Limited by the current of the compression motor, the external resistance can only vary from 40 Ω to 110 Ω.

Figs. 11 and 12 give the dependence of net acoustic power generated and thermal efficiency on the external resistance, respectively. The experiment results and the simulation results have a similar trend. However, there is a large deviation between the experiment results and simulation results. Especially for the thermal efficiency, in the experiment the thermal efficiency is quite small and less than 10%. It indicates that the heat input through the heater might have an even larger deviation between experiments and simulations.

Fig. 13 shows the volume flow rate amplitudes at the compressor outlet and at the expansion motor inlet. Fig. 14 shows the pressure amplitudes at these two positions. These two positions can also be approximately considered as the inlet and outlet of the tested THE unit. Since the piston displacement of the expansion motor is set as 6 mm, the volume flow rate at the expansion motor side is independent on external resistance. In Fig. 13 we could see that the experimental results of the volume flow rate amplitude is close to the simulation results. However, in Fig. 14, it is noticeable that the pressure amplitude drop from the compressor side to expansion motor side is much larger in the experiments than in the simulations. That's mainly because in the simulations, we simplify the special-shaped heater as a shell-and-tube heat exchanger so that the losses are much smaller.

There are some possible reasons that caused the large deviation between the experimental results and simulation results. Some possible ways to reduce the deviation are discussed here.

1. The structure of the heater has caused a very large flow loss and pressure drop. According to Fig. 14, the pressure drop in the experiment is much larger than that in the simulation. That means the pressure drop in the heater is much larger than expected. The sudden change of cross-sectional areas from a large tube to several small tubes will cause significant turbulence in the heater. Hence the acoustic power is terribly consumed in the heater. However, in the simulation, this loss is ignored to a large extent. By adding some rectifiers at the outlet of the heater may find help to suppress the turbulence to some extent.
2. The large deviation is mainly because of the heat loss and low heat absorption efficiency of the heating system. The total input electric power of the six silicon carbide heating rods is considered as the amount of the heat input into the system. However,

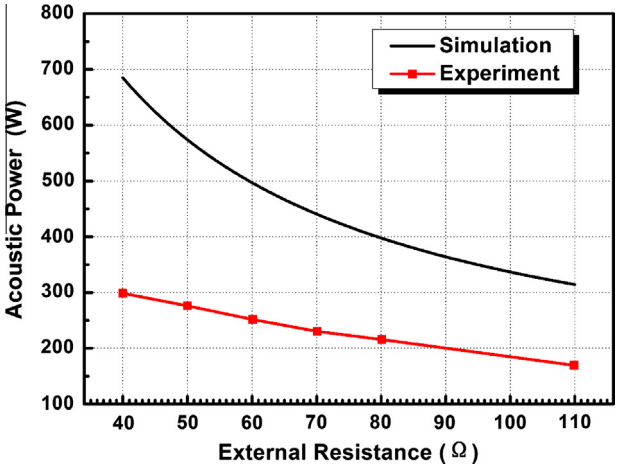

Fig. 11. Comparison between numerical and experiment: acoustic power.

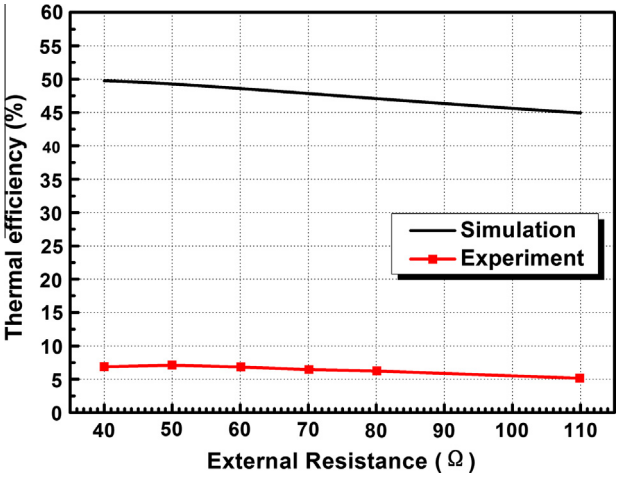

Fig. 12. Comparison between numerical and experiment: thermal efficiency.

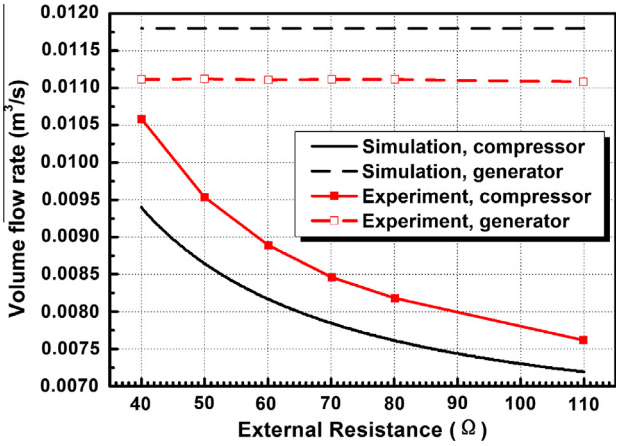

Fig. 13. External resistance versus volume flow rate.

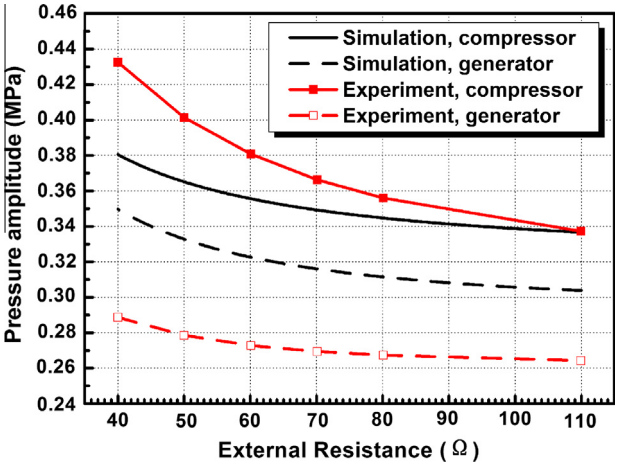

Fig. 14. External resistance versus pressure amplitude.

the practical heat used by the test rig is much less though it is difficult to determine how much energy is actually used by the system. First, about 30% of the length of the rods is not insulated in the Polycrystalline mullite for circuit connection. That means at least 30% of the heat radiation from the rods is wasted. Second, the radiation efficiency is limited by the confinement of the surface temperature of the rods, the radiation angle and the surface gray level of the heater. This results in a large temperature difference between gas and solid, thereby resulting in a large amount of heat wasted, more than 50%. Fig. 15 shows an infrared photo of the basic unit when it is heated. Fig. 16 shows the temperature variation with the external resistance. The temperature of the heater on the regenerator side is set as 650 °C approximately. The temperature of the gas in the heating chamber and the solid temperature of the hot end of the regenerator are also given in the figure. From Fig. 16 we can learn that the heat leak is very serious. The gas temperature in the heating chamber varies from 810.6 to 889.3 °C while the heater solid temperature is only 650 °C. Only 1949 W heat input is needed to maintain the solid temperature of the heater at 650 °C when the test rig is not working. While when the test rig is working, the heat input is 4341 W with an external resistance of 40 Ω. Based on the above analysis, about 50% of the heat is lost because of the heat leak. Third, the sudden change of cross-sectional areas from the heater to the thermal buffer tube will cause a jet-flow in the thermal buffer tube. This jet flow will cause heat losses through the thermal buffer tube. All these factors causes the serious heat leakage. Since the heat leak is so serious, much more heat should be input to maintain the temperature of heater. The thermal efficiency will have a terribly decrease consequently.

To solve this problem, some methods can be adopted. First, a better heating method such as heating through conduction should be considered. Second, a better insulation is necessary. Third, some meshes can be located at the inlet of the thermal buffer tube to suppress the jet-flow. Also the diameter of the heater tubes should be optimized.

3. Fig. 16 also reveals that there is a large temperature difference between the heater solid and regenerator solid. We set the solid temperature of the heater as 650 °C. In the simulations, the gas temperature at the high temperature side of the regenerator is near 650 °C since the heat transfer is relatively ideal. However, in the experiments, due to the abrupt change of the cross-sectional area from the regenerator to heater, the flow at this interface is quite complicated. The gas temperature at the high temperature side of the regenerator is much lower than 650 °C, having a 100–150 °C temperature difference. With a much smaller temperature gradient in the regenerator, the acoustic power generated is smaller.

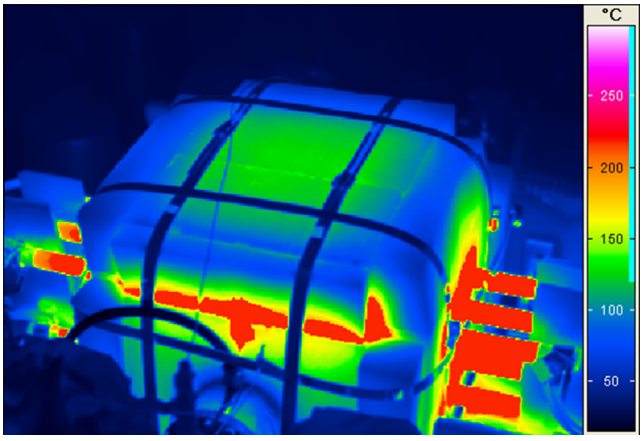

Fig. 15. The infrared photo of the basic unit when heating.

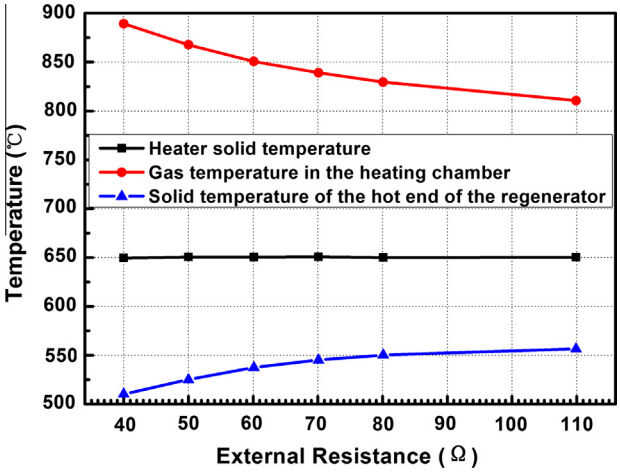

Fig. 16. External resistance versus temperature.

Generally speaking, the simulation is based on the ideal conditions to a large extent. Although there is a large deviation between the calculations and the experiments, the trends are coincident. Moreover, there is still large room for the experimental results improvement. Although some issues are left, the system shows its potential for application in solar power generation.

5. Conclusions

In this paper, a 6 × 1 kW double-acting THE is considered for a further application to drive generators to fulfil the dish-solar power generation. A basic unit which is representative to the whole system is numerically and experimentally studied. Some conclusions are drawn as follows.

1. The performance of the test rig was theoretically predicted. By adjusting the external resistance and moving mass of the expansion motor, the acoustic filed in the THE can be regulated to fulfil better energy conversion. A highest thermal efficiency of 51.37% and a net acoustic power of 1.6 kW under a heating temperature of 650 °C have been obtained with suitable external resistance and moving mass.
2. The heater parameter has a large influence on the performance of the basic unit.
3. Experiments have been conducted and the experimental results have been compared with the calculated results. Though some issues are still left, the system show its potential for an application for electric generation. Some improvements can be made to enhance the experimental results, such as improving the insulation, finding better ways to heat and adding some rectifier or meshes.

The further optimization and improvement of the heater will be carried out in near future to improve the thermal performance of the test rig.

Acknowledgments

This work was financially supported by the National Natural Sciences Foundation of China (51276186), the Major State Basic

Research Development Program of China (2010CB227303), and Beijing Natural Science Foundation (3132034).

References

[1] Swift G. Thermoacoutic engines. J Acoustical Soc Am 1988;84:1145–80.
[2] Ceperley P. Gain and efficiency of a short traveling wave heat engine. J Acoustical Soc Am 1985;77:1239–44.
[3] Ceperley P. A pistonless stirling engine – the traveling-wave heat engine. J Acoustical Soc Am 1979;66:1508–13.
[4] Yazaki T, Iwata A, Maekawa T, Tominaga A. Traveling wave thermoacoustic engine in a looped tube. Phys Rev Lett 1998;81:3128–31.
[5] Backhaus S, Swift G. A thermoacoustic stirling heat engine. Nature 1999;399:335–8.
[6] Luo EC, Ling H, Dai W, Zhang Y. A high-pressure ratio, energy-focused thermoacoustic heat engine with a tapered resonator. Chin Sci Bull 2005;50:284–6.
[7] Kees de Blok. Novel 4-stage travelling wave thermo-acoustic power generator. Proceedings of ASME 2010 3rd Joint US-European Fluids Engineering Summer Meeting and 8th International Conference on Nanochannels, Microchannels, and Minichannels, Montreal Canada; 2010, p. 30527.
[8] Swift G. Thermoacoustic natural gas liquefier. DOE Natural Gas Conference, Houston US; 1997. p. 1–5.
[9] Chen B, Yousif A, Riley P, Hann D. Development and assessment of thermoacoustic generators operating by waste heat from cooking stove. Engineering 2012;4:894–902.
[10] Luo EC, Hu JY, Dai W, Wu ZH, Yu GY, Li HB. A double-acting multi-stage travelling-wave thermoacoustic system (in Chinese). Chinese Invention Patent; 201110101963.
[11] Ward B, Clark J, Swift G. Design environment for low-amplitude thermoacoustic energy conversion, DELTAEC Version 6.2 Users Guide. Los Alamos: Los Alamos National Laboratory; 2008.
[12] Swift G. Thermoacoustics: a unifying perspective for some engines and refrigerators. New York: AIP Press; 2002.